Magnetic Phase Diagram of $La_{1-x}Sr_xCoO_3$ ($0 \leq x \leq 0.5$)

Spin-Glass Behavior and Magnetic Phase Diagram of $La_{1-x}Sr_xCoO_3$ ($0 \leq x \leq 0.5$) Studied by Magnetization Measurements

Masayuki ITOH, Ikuomi NATORI, Satoshi KUBOTA[1]
and Kiyoichiro MOTOYA[1]

Department of Physics, Faculty of Science, Chiba University,
Yayoi-cho, Inage-ku, Chiba 263
[1]Department of Physics, Faculty of Science, Saitama University,
Urawa, Saitama 338

(Received)

Abstract

Magnetic properties of $La_{1-x}Sr_xCoO_3$ ($0 \leq x \leq 0.5$) have been studied by magnetization measurements in low magnetic fields. It has been found that there exist spin-glass ($0 < x \lesssim 0.18$) and cluster-glass ($0.18 \lesssim x \leq 0.5$) regions. Ferromagnetic long-range order previously reported does not take place. Spin-glass behavior is ascribed to the frustration of random competing exchange interactions, namely the ferromagnetic double-exchange interaction between Co^{3+} and Co^{4+} and the antiferromagnetic one between like spins.

KEYWORDS: spin glass, cluster glass, magnetic phase diagram, magnetization, $La_{1-x}Sr_xCoO_3$

§1. Introduction

To elucidate the properties of strongly correlated electron systems many works on the electronic structure of 3 d transition metal oxides and metal-insulator transition by carrier doping have been made. Recently, $LaCoO_3$ and $La_{1-x}Sr_xCoO_3$ have been studied in connection with the spin-state transition by means of soft-x-ray-absorption (XAS)[1] and electron spectroscopies.[2] It has been revealed that $LaCoO_3$ is in the highly mixed character region between Mott-Hubbard and charge-transfer insulators. This finding is expected to provide new information to understand characteristic magnetic properties of these materials.

$LaCoO_3$ has been extensively studied in connection with the spin-state transition.[1-8] This compound is a semiconductor with a conductivity gap of ~0.6 eV,[2] and has a rhombohedrally distorted perovskite structure. The most characteristic feature of magnetic properties is the unusual temperature dependence of magnetic susceptibility. The susceptibility shows an abrupt decrease bellow ~100 K, a broad maximum and a gradual reduction obeying approximately a Curie-Weiss law at higher temperatures.[3-6] The maximum was found not due to the onset of a magnetic long-range order by no observation of magnetic Bragg peaks bellow 100 K in neutron scattering measurements.[7] The characteristic feature of magnetic properties was explained by a model of the thermally populated high-spin state $^5T_2$ ($t_{2g}^4e_g^2$) located at approximately 0.01-0.08 eV above the low-spin state $^1A_1$ (t_{2g}^6) for the trivalent cobalt ion.[3-6] The recent neutron scattering experiment also showed the temperature-induced cobalt magnetic moments which are explained by a thermally populated

high-spin model.[8] Furthermore, $La_{1-x}Sr_xCoO_3$ has also been extensively investigated.[9-14] The effect of Sr doping is known to introduce a ferromagnetic long-range order even for small doping of $x=0.01$ and itinerant ferromagnetism for $x>0.2$. Nevertheless, it seems that such magnetic properties have not been satisfactorily explained up to now. Randomness and frustration which come from the change of the spin state due to the hole doping should be properly taken into account for the study of the present system.

We have made a detailed and careful study on magnetic properties of $La_{1-x}Sr_xCoO_3$ ($0\leq x\leq 0.5$) by magnetization measurements in low magnetic fields using a SQUID magnetometer. In the present study, we have confined ourselves to the Sr concentration range $0\leq x\leq 0.5$, because the oxygen deficiency is known to increase above $x\sim 0.5$, if samples are not prepared under high oxygen pressures.[13,14] In this study, we confirmed that the ferromagnetic behavior previously reported is not due to a ferromagnetic long-range order but spin-glass freezing. We present a new magnetic phase diagram of $La_{1-x}Sr_xCoO_3$ ($0\leq x\leq 0.5$).

§2. Experimental Procedure

$La_{1-x}Sr_xCoO_3$ polycrystalline samples used in present experiments were prepared by a solid state reaction method. The appropriate mixture of La_2Co_3 (4N), $SrCO_3$ (4N) and CoO (4N) was ground and calcined at 950 °C for two days, and fired at 1300 °C for about 10 days with about 10 intermediate grindings. Finally it was slowly cooled (about 100 °C/day) from 950 °C to room temperature in air. The samples were confirmed to be of a single

phase with the rhombohedrally distorted perovskite structure by powder x-ray diffraction analysis. Magnetization measurements were done by using a SQUID magnetometer (Quantum Design, model MPMS).

§3. Experimental Results and Discussion

3.1 $LaCoO_3$

Figure 1 shows the temperature dependence of magnetic susceptibility χ taken at 55 kOe. The result essentially agrees with the previous data.[4,5] Bellow ~25 K, χ follows the formula $\chi=C/(T-\Theta)+\chi_0$ with the Curie constant $C=1.50\times10^{-4}$ K·emu/g, the Weiss constant $\Theta=-28.8$ K and $\chi_0=2.07\times10^{-6}$ emu/g. The recent NMR measurements[15] have shown that the Curie-Weiss behavior at low temperatures is not an intrinsic character. The temperature independent susceptibility χ_0 due to Van-Vleck orbital paramagnetism shows the nonmagnetic low-spin state $^1A_1$ as the ground state. Above ~25 K, χ increases rapidly with increasing temperature and exhibits a broad maximum at ~100 K as reported previously. To explain these characteristic features of χ, the recent XAS study[1] provides a useful information on the spin-state transition of a trivalent cobalt. That is, $LaCoO_3$ is in a highly covalent low-spin state of $^1A_1$ up to ~420 K and exhibits a gradual transition to a mixed-spin state of the low-spin state and a high-spin one of $^5T_2$ at higher temperatures 420-650 K. Therefore, it is sufficient to take into account only the two-level population of the nonmagnetic ground $^1A_1$ (S=0) and the excited $^5T_2$ (S=2) states for understanding the broad maximum of χ at ~100 K as the previous analysis.[6,16,17]

3.2 Spin-glass region ($0 < x \lesssim 0.18$)

A doping of Sr bellow x_c~0.18 introduces several changes in magnetic properties as mentioned bellow.

Figure 2 shows the temperature dependence of magnetization M(T) for x= 0.06, 0.09, 0.12 and 0.15. These data were taken in a field of 20 Oe after cooling from room temperature to the lowest temperature in a field of 20 Oe (FC) or in zero field (ZFC). In $M_{FC}(T)$ curves, a kink or plateau appears at T_g= 15 K (x=0.06), 33 K (x=0.09), 49 K (x=0.12) and 65 K (X=0.15), whereas a cusp is seen at T_g in $M_{ZFC}(T)$ curves, as is usually observed in spin-glass systems. T_g monotonously increases with increasing Sr concentration. The difference between $M_{FC}(T)$ and $M_{ZFC}(T)$ persists up to ~200 K in all samples.

Magnetization curves M(H) taken after ZFC in fields up to 30 kOe are presented for x=0.15 in Fig. 3. At 5 K well bellow T_g~65 K, the M(H) curve after ZFC is of a characteristic S shape. On the other hand, the M(H) curve at 65 K shows the presence of nonlinear susceptibility. These behavior of M(H) is also one of the characteristic features in spin-glass systems.[18)]

We have observed a long-time nonexponential relaxation behavior of $M_{ZFC}(t)$ for x=0.09. The experimental procedure is as follows. After the ZFC process from room temperature to 6 K ($< T_g$), the sample was maintained in zero field for different waiting times t_w=0, 30 and 300 min before application of a field of 100 Oe. As soon as the field was applied at time t=0, we measured magnetization $M_{ZFC}(t)$ as a function of time t. Figure 4 shows the M_{ZFC} vs. log(t) plot for x=0.09. The M_{ZFC} vs. log(t) plot has an inflection point at the time near the waiting time

t_w. This situation is more clearly seen in the $dM_{ZFC}/d\ln(t)$ vs. $\log(t)$ plot as shown in Fig. 5. The relaxation rate $dM_{ZFC}/d\ln(t)$ has a broad maximum at about t_w which is denoted by arrows for t_w= 30 and 300 min in Fig. 5. This characteristic behavior of $M_{ZFC}(t)$ is called the aging effect which was reported in other spin-glass systems.[19,20] Within the droplet scaling theory the aging effect is ascribed to the thermally activated growth of spin-glass-ordered domains.[21]

Therefore, the experimental results mentioned above clearly reveal the onset of the spin-glass freezing at T_g in the Sr concentration range $0<x\lesssim 0.18$. At present, however, we can not clarify the origin of the difference between M_{FC} and M_{ZFC} observed even well above T_g.

3.3 Cluster-glass region ($0.18 \lesssim x \leq 0.5$)

Further increasing Sr concentration over x_c~0.18 introduces a magnetic phase different from the spin-glass phase.

As is shown in Fig. 6, M rapidly increases with increasing x from 0.15 to 0.2. M_{FC} at 20 Oe for x=0.2 shows a gradual increase bellow T_s~180 K, whereas M_{ZFC} at 20 Oe deviates from M_{FC} bellow T_s and shows a broad maximum around ~160 K. Similar behavior is seen for x=0.3, 0.4 and 0.5 as presented in Fig. 6. M_{FC} for x=0.5, for example, rapidly increases in the temperature range just bellow T_s~245 K and gradually does with further decreasing temperature, whereas M_{ZFC} exhibits a gradual reduction with decreasing temperature, following a pronounced increase near T_s~245 K and a peak at ~240 K. This large difference between M_{FC} and M_{ZFC} bellow T_s indicates no simple ferromagnetic long-range

order in this Sr concentration range.

M(H) was measured up to 55 kOe at several temperatures for x=0.5 as shown in Fig. 7. M at 6 K does not reach its saturation value even at 55 kOe, where magnetic moment per cobalt is 1.9 μ_B. As is shown in Fig. 8, Arrot plots of magnetization show a poor linear relation not observed in a simple ferromagnet, although the plots indicate the onset of spontaneous magnetization bellow T_s~245 K. Such poor linear relation was previously observed a little bellow T_s in the measurement of M(H) up to 10 kOe, although the measurement was analyzed on the basis of a ferromagnetic long-range order.[12)]

Another characteristic feature which indicates the absence of a ferromagnetic long-range order was also observed. Figure 9 shows the long-time relaxation of $M_{ZFC}(t)$ for three waiting times t_w= 0, 30 and 300 min in the x=0.5 sample, which was measured by the same procedure as mentioned in subsection 3.2. Also the corresponding relaxation rate $dM_{ZFC}(t)/dln(t)$ vs. log(t) for x=0.5 is presented in Fig. 10. Apparently, $M_{ZFC}(t)$ shows the long-time relaxation behavior not observed in ferromagnets. Furthermore, this long-time relaxation does not show such an aging effect observed in the spin-glass region.

In conclusion, samples in the Sr concentration region $0.18 \lesssim x \leq 0.5$ exhibit no long-range ferromagnetic order but show a cluster-glass behavior with the finite ferromagnetic spin correlation.

3.4 Magnetic phase diagram

On the basis of magnetization measurements mentioned above,

we constructed a magnetic phase diagram of $La_{1-x}Sr_xCoO_3$ ($0 \leq x \leq 0.5$) as shown in Fig. 11. In this figure, solid circles in the Sr concentration range $0 < x \lesssim 0.18$ correspond to temperatures T_g where the spin freezing takes place. On the other hands, solid circles for $0.18 \lesssim x \leq 0.5$ represent onset temperatures T_s of the cluster-glass phase at which spontaneous magnetization sets in with the finite ferromagnetic correlation. Magnetization measurements clearly indicate the presence of phase boundary between spin-glass and cluster-glass phases at $x_c \sim 0.18$.

Now, we will consider exchange interactions between cobalt spins. The substitution of Sr^{2+} for La^{3+} converts its nearest neighbor cobalts into the tetravalent low-spin Co^{IV} (t_{2g}^5), high-spin Co^{4+} ($t_{2g}^3 e_g^2$) or intermediate-spin ($t_{2g}^4 e_g^1$) state. However, the electron spectroscopy study indicated that the doped hole has the lowest energy for the high-spin Co^{4+} state which has an energy approximately 1 eV lower than those of the low-spin Co^{IV} and the intermediate-spin state.[2] Bellow ~300 K, therefore, it is sufficient to consider only the high-spin Co^{4+} which is strongly hybridized by the charge-transfer state. Other cobalts will remain in the trivalent low-spin state Co^{III} ($^1A_1$) having the high-spin Co^{3+} ($^5T_2$) state located at about 0.01-0.08 eV above the low-spin state. The ferromagnetic double-exchange interaction is considered to be predominantly present between such trivalent and tetravalent cobalt spins.[22,23] The exchange interaction $J_{Co^{4+}-Co^{III}}$ between Co^{4+} and Co^{III} is also estimated to be ferromagnetic owing to Goodenough and Kanamori's rule.[24] On the other hand, the superexchange interactions between high Co spins such as $J_{Co^{3+}-Co^{3+}}$ and $J_{Co^{4+}-Co^{4+}}$ are antiferromagnetic. Hence, we must

take account of randomness and competition between ferromagnetic and antiferromagnetic exchange interactions, which provide the spin-glass behavior observed for $0<x\lesssim 0.18$. When the ferromagnetic exchange interactions overcome the antiferromagnetic one, the cluster glass appears at x_c. Frustration in the boundary between ferromagnetic clusters appears because of competition between ferromagnetic and antiferromagnetic exchange interactions, consequently preventing a ferromagnetic long-range order. If the Sr doping further increases over x=0.5, a ferromagnetic phase should appear, which includes an itinerant ferromagnet $SrCoO_3$ with Curie temperature T_c= 222 K.[13]

As regards conducting properties, replacing La with Sr bellow x~0.2 introduces hole states above Fermi level E_F.[2] Further increasing Sr concentration over x~0.2 makes these doped hole states overlap E_F, and results in the metallic phase. This metal-insulator transition is considered to closely correlate to the onset of the cluster glass, because the double-exchange mechanism results in itinerancy of the d electron. Also it may be related to the percolation concentration x_p=0.31 calculated for the sc lattice with the nearest-neighbor interaction.[25]

§4. Conclusions

Magnetization measurements have been done to reveal in detail magnetic properties of $La_{1-x}Sr_xCoO_3$ ($0\le x\le 0.5$). We constructed a magnetic phase diagram with characteristic features mentioned bellow.

(1)$LaCoO_3$: The pronounced increase of χ was observed at

~100 K, corresponding to the thermally populated high-spin state of a trivalent cobalt ion.

(2)Spin-glass region ($0<x\lesssim 0.18$): M_{ZFC} shows a cusp at the spin-glass freezing temperature T_g. Also we have observed the long-time relaxation of M_{ZFC} having the aging behavior bellow T_g.

(3)Cluster-glass region($0.18\lesssim x\leq 0.5$): Spontaneous magnetization appears bellow T_s with the finite ferromagnetic correlation. The long-time relaxation of M_{ZFC} and the large difference between M_{FC} and M_{ZFC} bellow T_s clearly indicate that a simple ferromagnetic long-range order does not take place.

In particular, it should be noted that the ferromagnetic long-range order previously reported for the small doping region does not exist because of the frustration between ferromagnetic double-exchange and antiferromagnetic superexchange interactions.

References

1) M. Abbate, J. C. Fuggle, A. Fujimori, L. H. Tjeng, C. T. Chen, R. Potze, G. A. Sawatzky, H. Eisaki and S. Uchida : Phys. Rev. B 47 (1993) 16124.

2) A. Chainani, M. Mathew and D. D. Sarma : Phys. Rev. B 46 (1992) 9976.

3) P. M. Raccah and J. B. Goodenough : Phys. Rev. 155 (1967) 932.

4) G. H. Jonker : J. Appl. Phys. 37 (1966) 1424.

5) V. G. Bhide, D. S. Rajoria, G. Rama Rao and C. N. R. Rao : Phys. Rev. B 6 (1972) 1021.

6) C. S. Naiman, R. Gilmore, B. Dibartolo, A. Linz and R. Santoro : J. Appl. Phys. 36 (1965) 1044.

7) W. C. Koehler and E. O. Wollan : J. Phys. Chem. Solids, 2 (1957) 100.

8) K. Asai, P. Gehring, H. Chou and G. Shirane : Phys. Rev. B 40 (1989) 10982.

9) G. H. Jonker and J. H. Van Santen : Phyica 19 (1953) 120.

10) P. M. Raccah and J. B. Goodenough : J. Appl. Phys. 39 (1968) 1209.

11) V. G. Bhide, D. S. Rajoria, C. N. R. Rao, G. Rama Rao and V. G. Jadhao : Phys. Rev. B 12 (1975) 2832.

12) N. Menyuk, P. M. Raccah and K. Dwight : Phys. Rev. 166 (1968) 510.

13) H. Taguchi, M. Shimada and M. Koizumi : Mat. Res. Bull. 13 (1978) 1225.

14) H. Taguchi, M. Shimada and M. Koizumi : Mat. Res. Bull. 15 (1980) 165.

15) M. Itoh and I. Natori : in preparation for publication.

16) R. Zimmermann and E. König : J. Phys. Chem. Solids 38 (1977) 779.

17) M. Eibschütz, M. E. Lines and F. J. DiSalvo : Phys. Rev. B 15 (1977) 103.

18) K. Binder and A. P. Young. : Rev. Mod. Phys. 58 (1986) 801.

19) L. Lundgren, P. Svedlindh, P. Nordblad and O. Beckman : Phys. Rev. Lett. 51 (1983) 911.

20) P. Granberg, L. Sandlund, P. Nordblad, P. Svedlindh and L. Lundgren : Phys. Rev. B 38 (1988) 7097.

21) D. S. Fisher and D. A. Huse : Phys. Rev. B 38 (1988) 373.

22) P. W. Anderson and H. Hasegawa : Phys. Rev. 100 (1955) 675.

23) P. G. de Gennes : Phys. Rev. 118 (1960) 141.

24) J. B. Goodenough and J. M. Longo : Landolt-Börnstein, ed. K. H. Hellwege (Springer-Verlag, Berlin, 1970) New Series, Group III, vol. 4, p.126.

25) D. Stauffer : Introduction to Percolation Theory (Taylor & Francis, London, 1985) p.17.

Figure Captions

Fig. 1. Temperature dependence of magnetic susceptibility of $LaCoO_3$ taken at 55 kOe.

Fig. 2. Temperature dependence of magnetization at 20 Oe of $La_{1-x}Sr_xCoO_3$ (x= 0.06, 0.09, 0.12, and 0.15). Solid and open symbols represent field-cooled (FC) and zero-field-cooled (ZFC) magnetizations, respectively. Only the x=0.15 sample refers to the right vertical axis. Solid curves are drawn to guide the eye.

Fig. 3. Magnetization curves of $La_{0.85}Sr_{0.15}CoO_3$ at 5, 65 and 100 K. Solid curves are drawn to guide the eye.

Fig. 4. Time evolution of magnetization M_{ZFC} at 100 Oe after zero-field cooling from room temperature to 6 K for different waiting times t_w = 0, 30 and 300 min in $La_{0.91}Sr_{0.09}CoO_3$. Solid curves are drawn to guide the eye.

Fig. 5. Relaxation rate of magnetization $dM_{ZFC}/dln(t)$ vs. log(t) for different waiting times t_w = 0, 30 and 300 min in $La_{0.91}Sr_{0.09}CoO_3$. Solid curves are drawn to guide the eye.

Fig. 6. Temperature dependence of magnetization at 20 Oe of $La_{1-x}Sr_xCoO_3$ (x= 0.2, 0.3, 0.4 and 0.5). Solid and open symbols represent field-cooled (FC) and zero-field-cooled (ZFC) magnetizations, respectively. Solid curves are drawn to guide the eye.

Fig. 7. Magnetization curves of $La_{0.5}Sr_{0.5}CoO_3$ at 6, 200, 240, 245, 250 and 260 K. Solid curves are drawn to guide the eye.

Fig. 8. Arrot plots of magnetization curves of $La_{0.5}Sr_{0.5}CoO_3$ at 6, 200, 240, 245, 250 and 260 K. Solid curves are drawn to guide the eye.

Fig. 9. Time evolution of magnetization M_{ZFC} at 100 Oe after zero-field cooling from room temperature to 6 K for different waiting times t_w = 0, 30 and 300 min in $La_{0.5}Sr_{0.5}CoO_3$. Solid curves are drawn to guide the eye. Fig.10. Relaxation rate of Magnetization $dM_{ZFC}(t)/dln(t)$ vs. log(t) for different waiting times t_w = 0, 30 and 300 min in $La_{0.5}Sr_{0.5}CoO_3$. Solid curves are drawn to guide the eye.

Fig.10. Relaxation rate of magnetization $dM_{ZFC}/dln(t)$ vs. log(t) for different waiting times t_w = 0, 30 and 300 min in $La_{0.5}Sr_{0.5}CoO_3$. Solid curves are drawn to guide the eye.

Fig.11. Magnetic phase diagram of $La_{1-x}Sr_xCoO_3$ ($0 \leq x \leq 0.5$). SG, CG and P represent spin-glass, cluster-glass and paramagnetic phases, respectively. The boundary between SG and CG is located at x~0.18 as is shown by the dashed line. The solid curve is drawn to guide the eye.

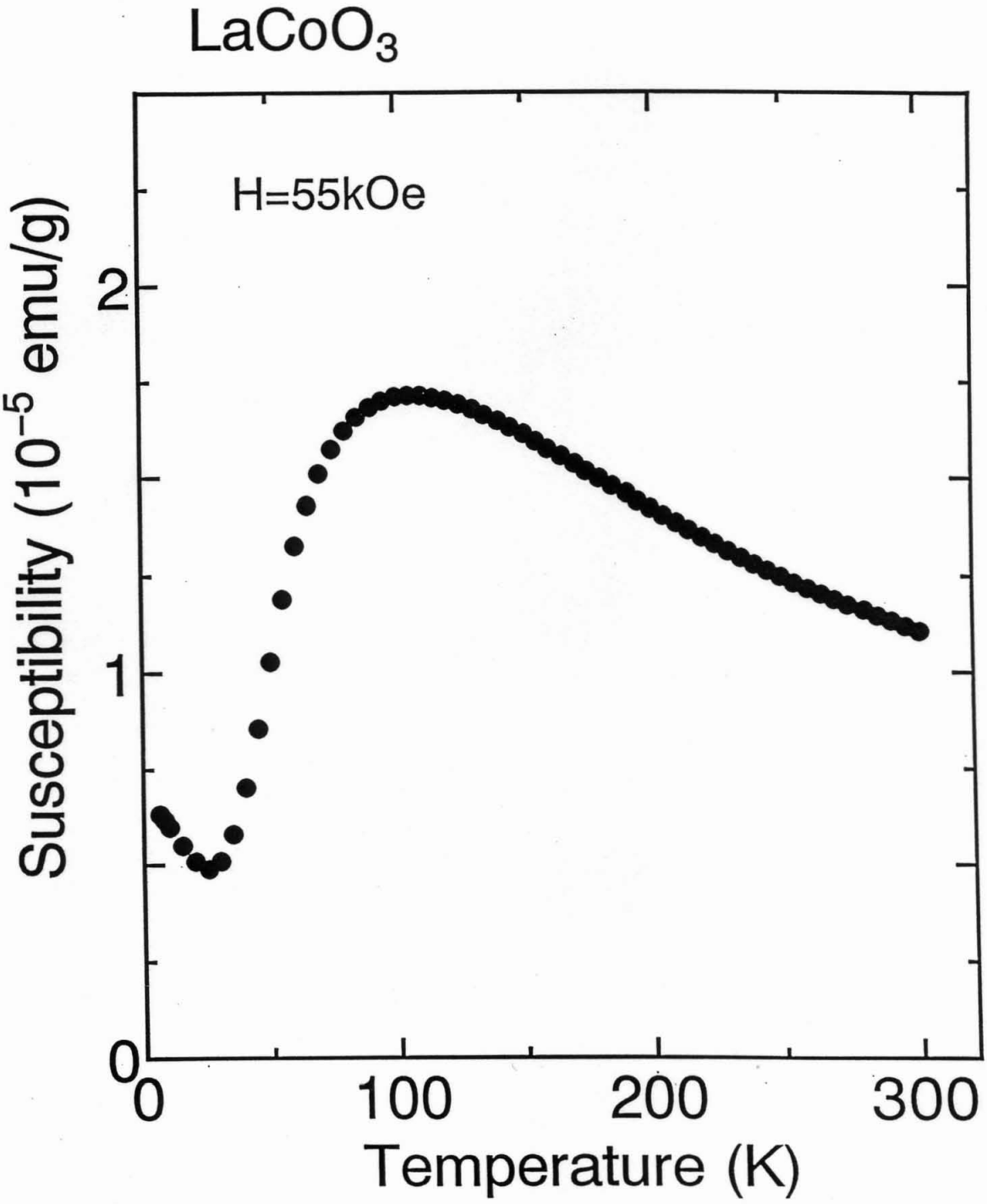

Fig.1 M.Itoh et al. ⑦

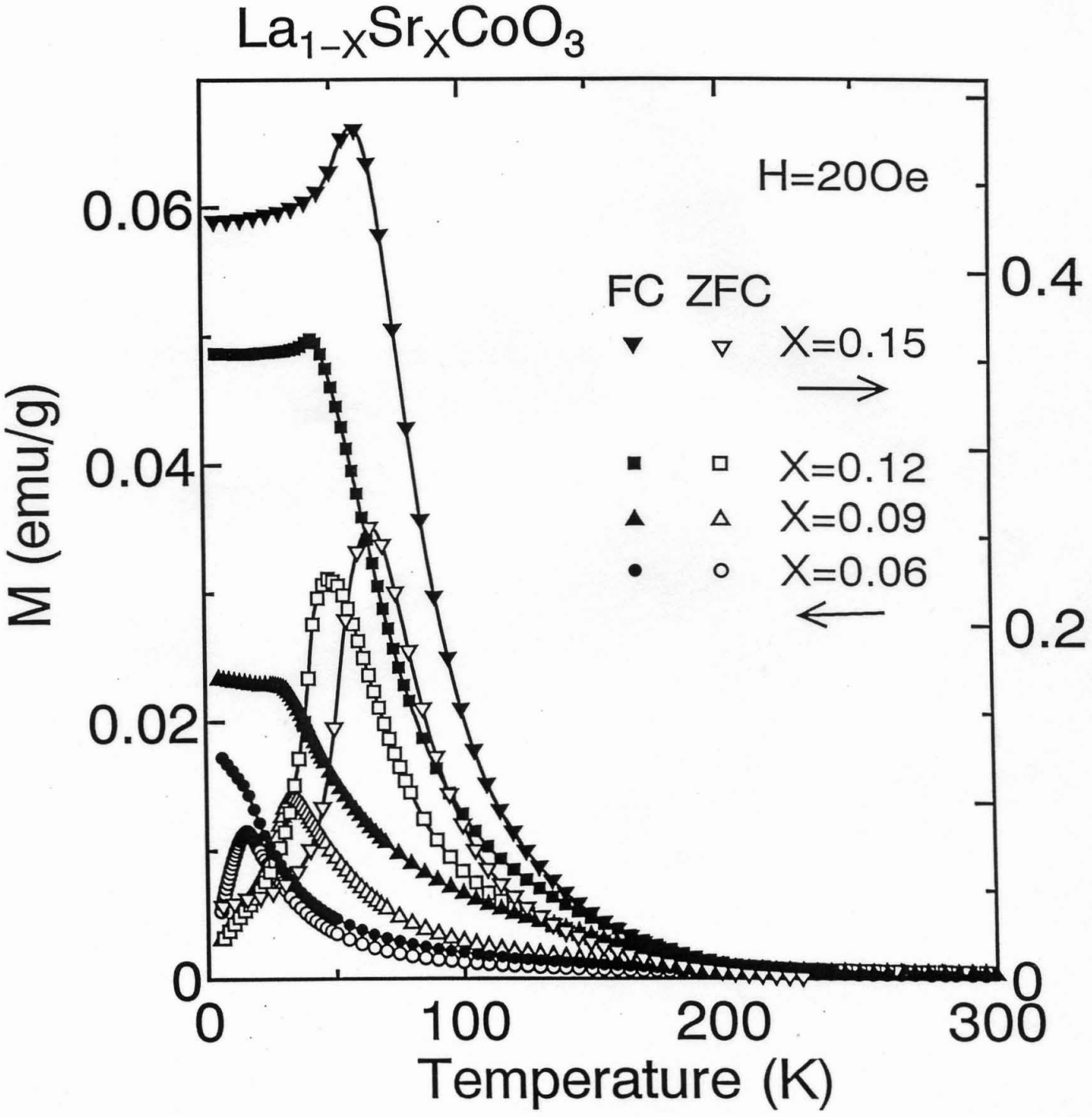

Fig.2 M.Itoh et al. ⑦

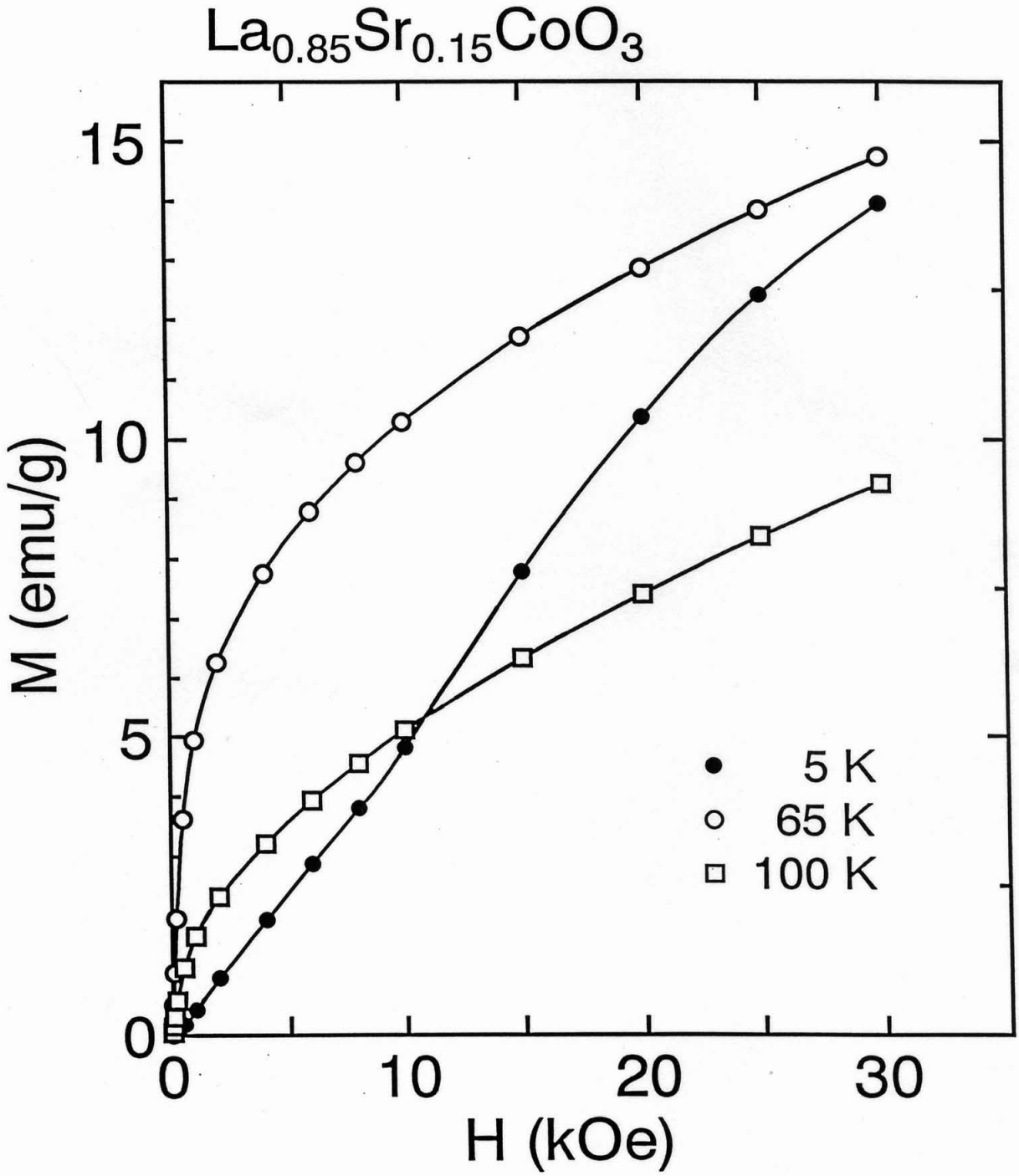

Fig.3 M.Itoh et al. ⑦

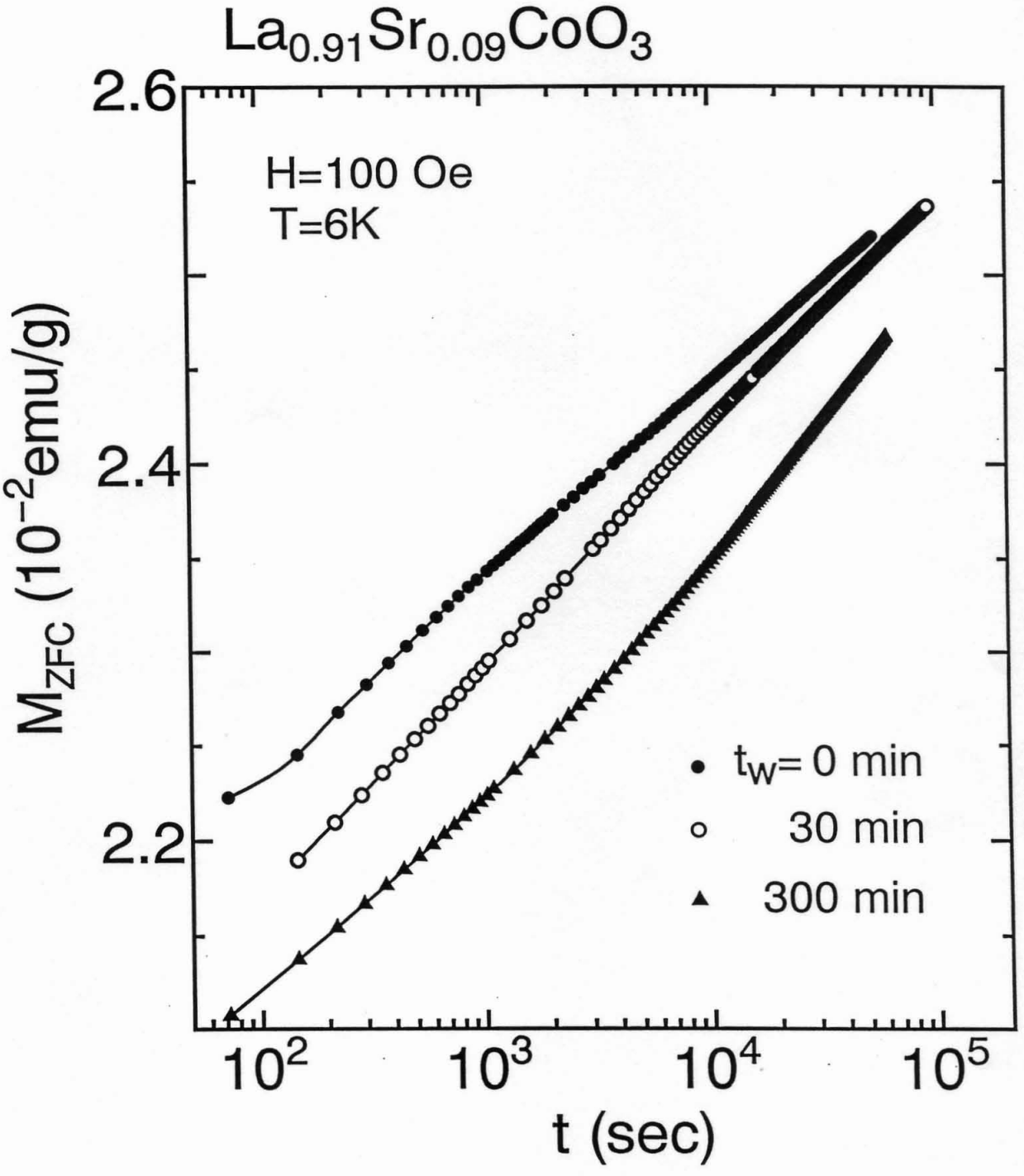

Fig.4 M.Itoh et al. ⑦

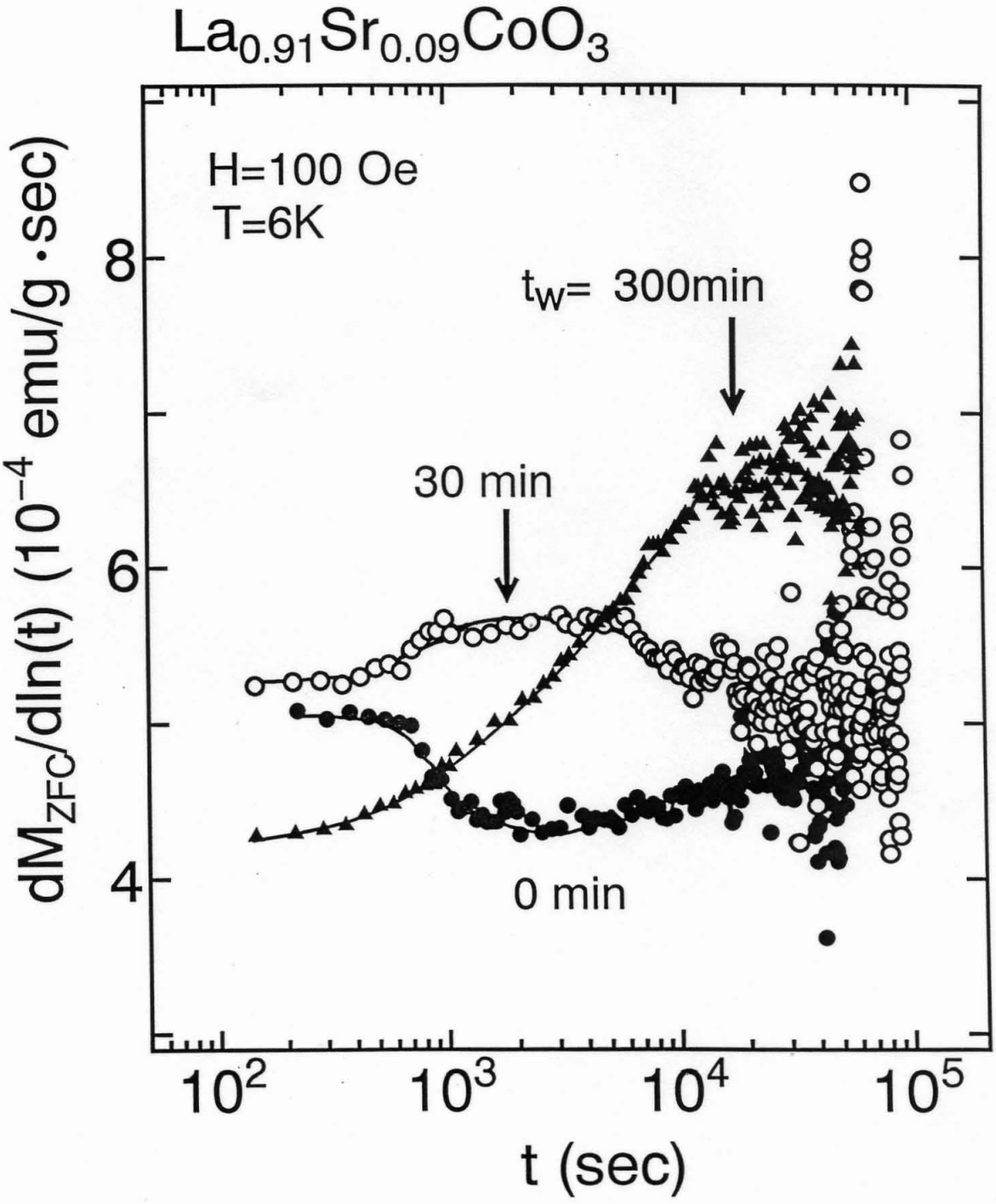

Fig.5 M.Itoh et al. ⑦

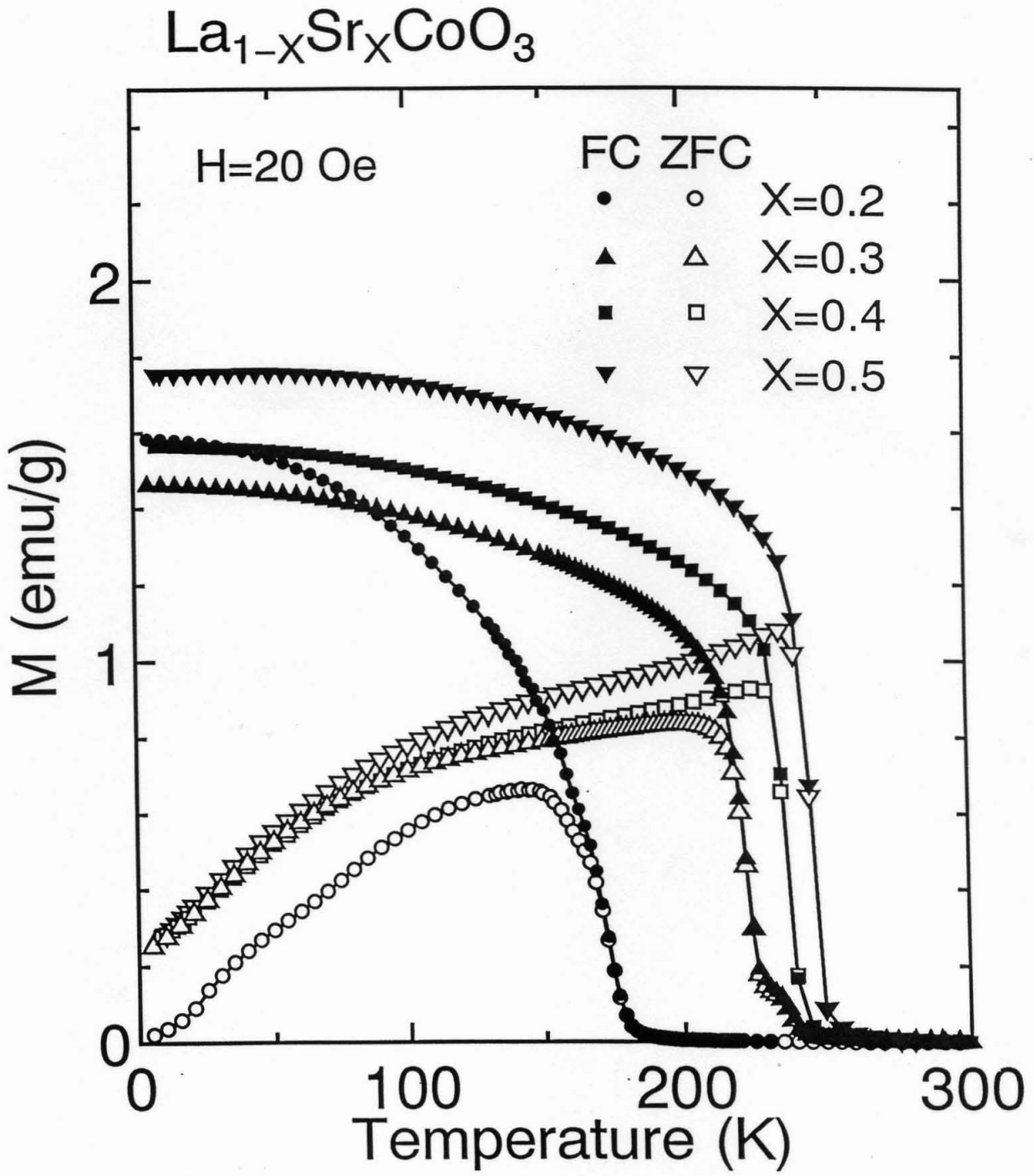

Fig.6 M.Itoh et al. ⑦

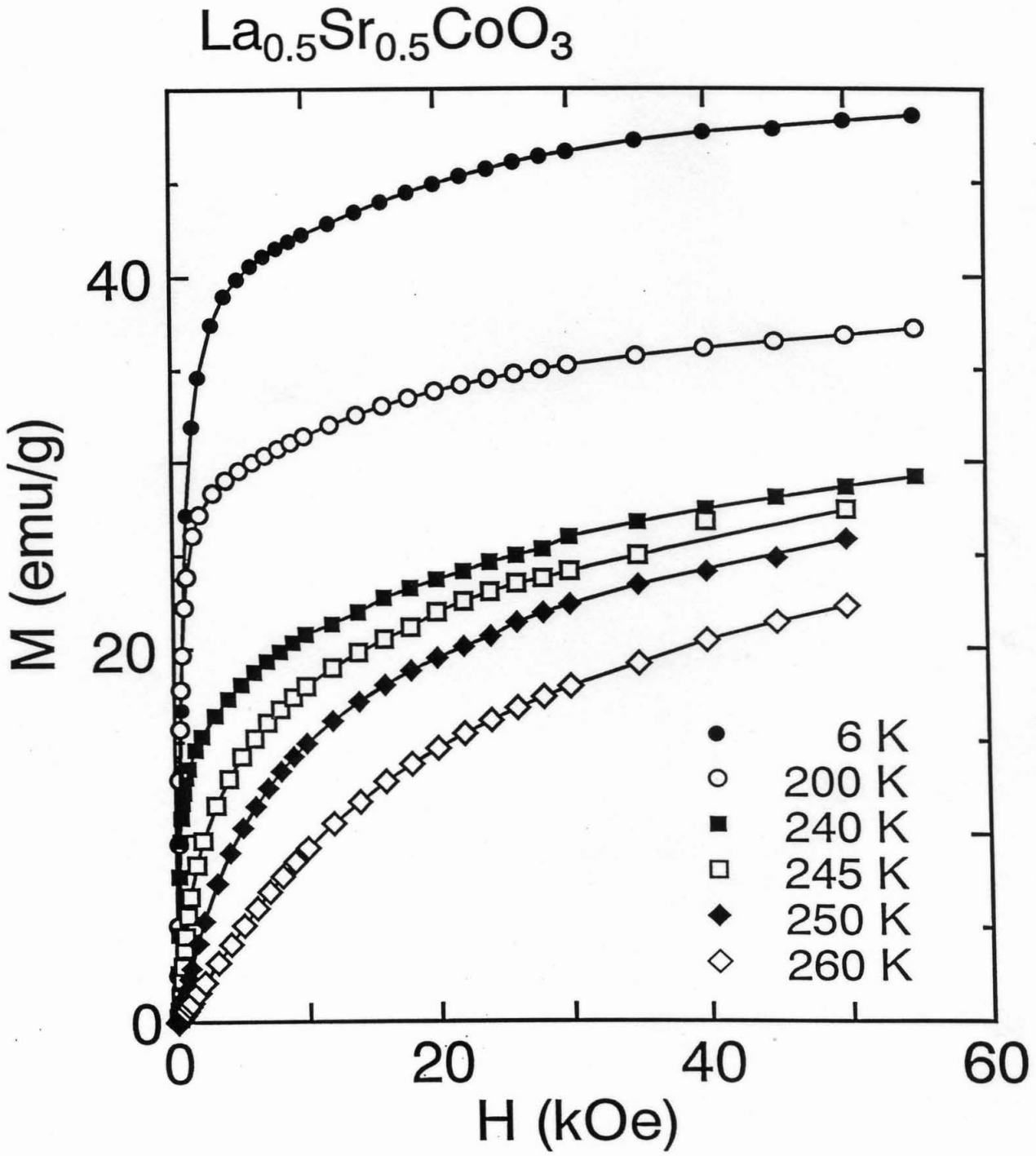

Fig.7 M.Itoh et al. ⑦

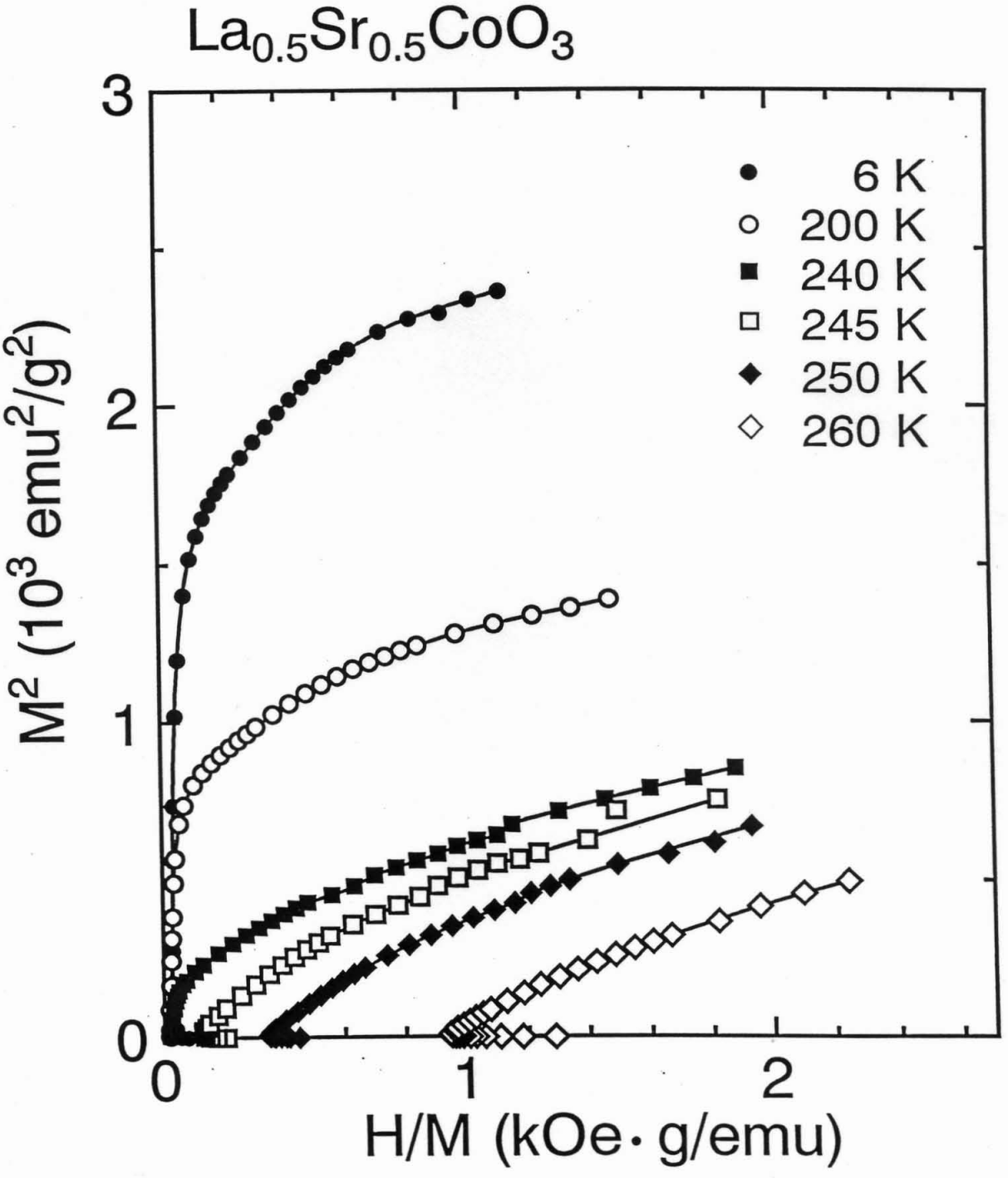

Fig.8 M.Itoh et al. ⑦

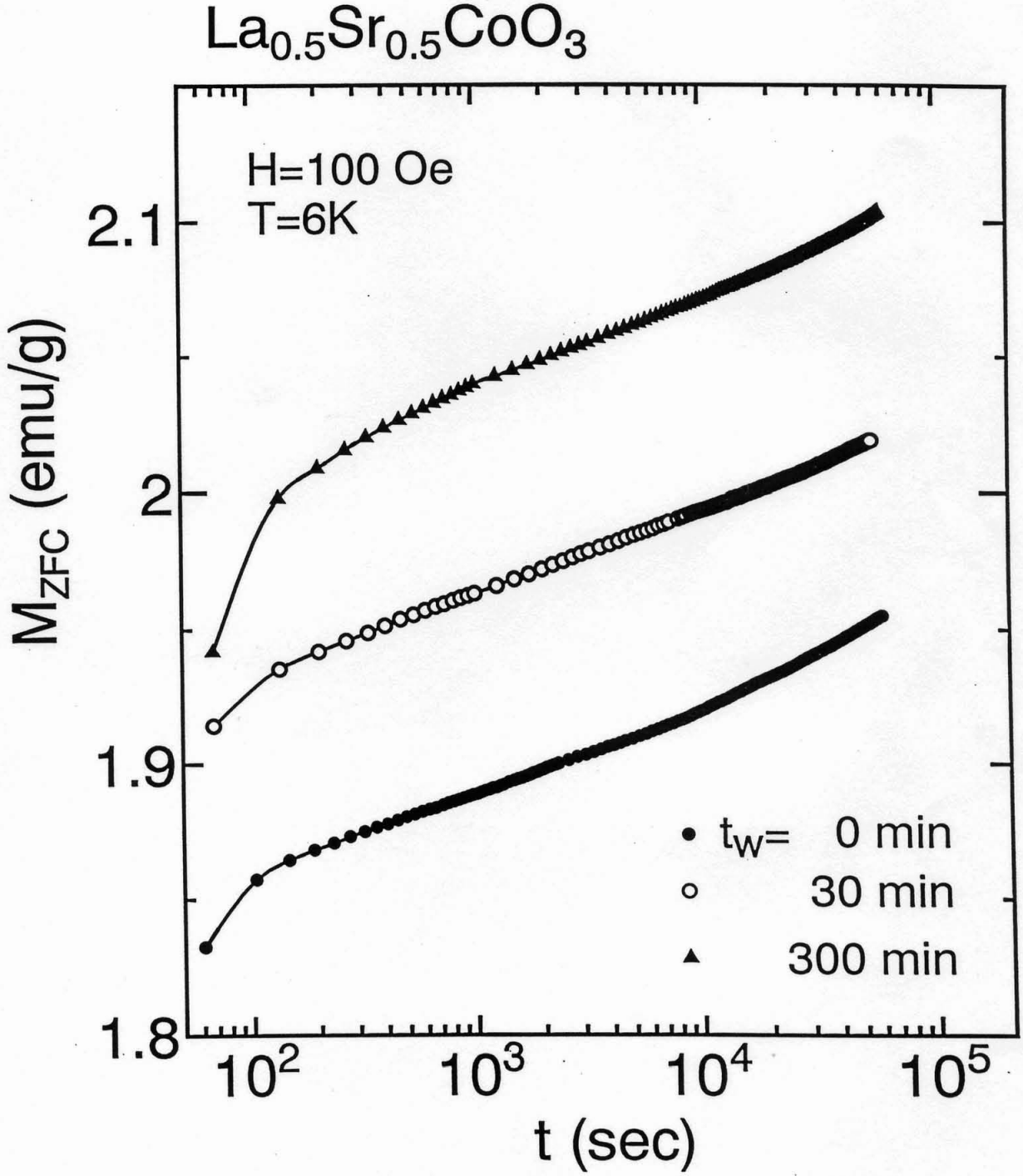

Fig.9 M.Itoh et al. ⑦

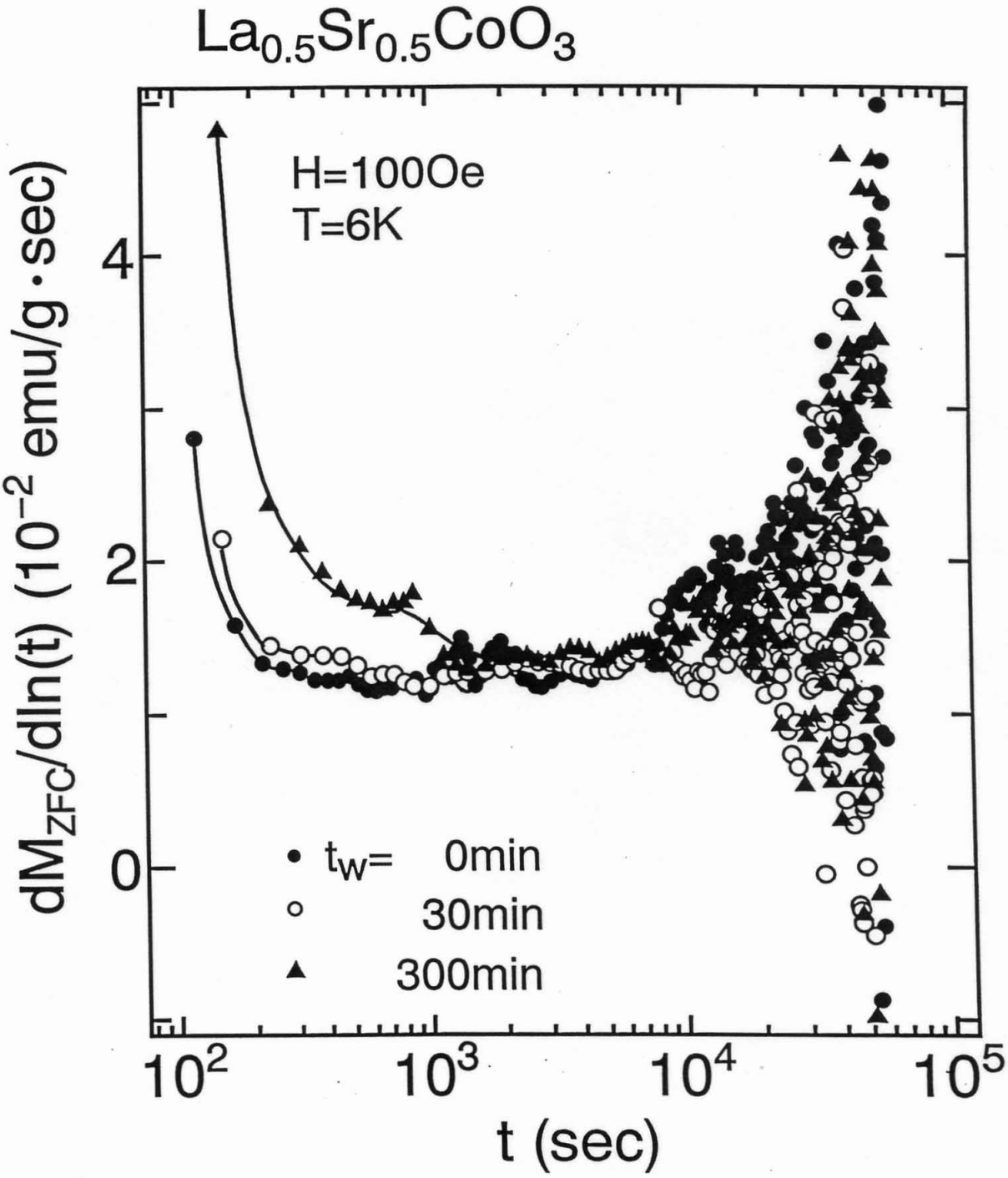

Fig.10 M.Itoh et al. ⑦